IU ST
Iran University of Science and Technology

Iranian Journal of Electrical and Electronic Engineering

Journal Homepage: ijeee.iust.ac.ir

Cost Optimization and Battery Sizing of Grid-Connected Microgrid with Distributed Energy Resources Using Random Forest Technique

J. Vaish*(C.A.), A. Kumar Tiwari** and Seethalekshmi K.***

Abstract: In recent years, Microgrids in integration with Distributed Energy Resources (DERs) are playing as one of the key models for resolving the current energy problem by offering sustainable and clean electricity. Selecting the best DER cost and corresponding energy storage size is essential for the reliable, cost-effective, and efficient operation of the electric power system. In this paper, the real-time load data of Bengaluru city (Karnataka, India) for different seasons is taken for optimization of a grid-connected DERs-based Microgrid system. This paper presents an optimal sizing of the battery, minimum operating cost and, reduction in battery charging cost to meet the overall load demand. The optimization and analysis are done using meta-heuristic, Artificial Intelligence (AI), and Ensemble Learning-based techniques such as Particle Swarm Optimization (PSO), Artificial Neural Network (ANN), and Random Forest (RF) model for different seasons i.e., winter, spring & autumn, summer and monsoon considering three different cases. The outcome shows that the ensemble learning-based Random Forest (RF) model gives maximum savings as compared to other optimization techniques.

Keywords: Artificial Neural Network (ANN), Battery Energy Management System (BESS), Distributed Energy Resources (DERs), Microgrid, Particle Swarm Optimization (PSO), Random Forest (RF)

1 Introduction

THE energy demand is significantly impacted by the lack of fossil fuels, and day by day it is getting harder to supply the expanding energy needs of economies and populations. The price of energy increases as a result of the depletion of fossil fuels, which is one of the main repercussions. Finding and developing alternative energy sources, such as Renewable Energy Sources (RESs) including solar, wind, and hydropower, etc., becomes more crucial [1]-[2]. To cut carbon emissions and make the transition to a more sustainable energy future, it has become more crucial in recent years to discuss the integration of RESs, like as wind and solar electricity, into the grid system. The traditional grid system is being changed into a "smart Microgrid (MG)" to enable this transformation.

These Microgrid (MG) systems may efficiently integrate and control these Distributed energy sources (DERs) [3]-[5] to satisfy local energy needs, ensuring the microgrid system's dependability, efficacy, and cost-effectiveness. One of the key challenges of incorporating renewable energy into the Microgrid (MG) system is the variability of these sources [6]-[8]. To overcome this difficulty, energy storage systems like batteries and flywheels can be utilized to store extra energy produced during periods of shortages and discharge it during periods of increased demand [9]-[11].

Further, the use of BESS in MG helps to reduce energy costs, careful planning and management. This includes selecting the appropriate battery technology and capacity, installing monitoring and control systems to regulate the energy flow, and integrating the BESS with the local

Iranian Journal of Electrical & Electronic Engineering, 2023.
Paper first received 06 June 2023 and accepted 12 December 2023.
* The author is with Department of Electronics and Communication, Amity University Uttar Pradesh, Lucknow Campus, U.P., India
E-mail: itayaj26@gmail.com.
** The author is with Department of Electrical and Electronics, Amity University Uttar Pradesh, Lucknow Campus, U.P., India
E-mail: akumar3@lko.amity.edu
*** The author is with Department of Electrical Engineering, Institute of Engineering and Technology, Lucknow Campus, U.P., India
E-mail: seethalekshmik@ietlucknow.ac.in
Corresponding Author: J. Vaish.

distribution network and other DERs. Also, several studies and analyses are done for optimal sizing and charging and discharging of batteries when RESs are also considered in MG [12]-[15]. Different control algorithms and optimization techniques have been developed to maximize earnings, depending on the market regulations and bids for energy reserves. The suggestion is to combine two or more renewable energy sources with storage for high levels of renewable energy penetration. Some cutting-edge techniques involve setting up distributed storage on a microgrid while maximizing their placement and size using various optimization techniques, strategies, and collaborative algorithms [16]-[18].

In the last few decades, the literature has offered a range of metaheuristic optimization strategies for resolving the sizing and minimizing the cost problem of the MG system. These kinds of strategies are being studied by researchers more and more because of how well they can tackle challenging optimization issues. However, these optimization techniques do not guarantee an absolute optimal solution to a complex problem. Also, the time required for finding a "near-optimal" solution can be large in an unlucky case. Thus, the convergence problem and accuracy and convergence time of each technique's performance, however, may vary when used for the size optimization [19]-[21]. The literature has also covered a variety of scaling methods, including iterative methods [22]– [23] and software tools like HOMER [24]– [26]. The usage of traditional procedures based on iterative, numerical, or analytical methods has significantly decreased because of their delayed reaction and results [27]-[31]. Recently, due to the advancement in AI tools, machine learning (ML)-based optimization models have been implemented in MG for fast convergence and more accurate results on non-linear data. Numerous studies have examined the use of such algorithms to address the size problem facing renewable energy systems [32] - [34]. The process of ML optimization aims to lower the risk of errors or loss from these predictions and improve the accuracy of the model. Machine learning models are often trained on local or offline datasets which are usually static. ML Optimization improves the accuracy of predictions and classifications and minimizes error.

The novelty of this research is that the real-time load data of Bengaluru City (Karnataka, India) from 1st January 2022 to 31st December 2022 is considered for MG optimization using the RF model. Also, the constraint of charging batteries from RES from 12:00 noon to 6:00 noon is taken into account to meet the load demand. Few studies have examined and explored grid-connected MG system optimization using machine learning techniques until now. Researchers choosing an MG system for their sizing and scheduling might utilize the assessment presented in this case study as a useful reference.

In this paper, the main objectives covered include:

(i) The mathematical modeling of grid-connected microgrids with Distributed Energy Resources (DERs) has been examined. The effectiveness of the system is assessed using this MG model. Real-time meteorological information on wind speed and solar radiation is also taken into account for accuracy.

(ii) The evaluation and determination of optimal battery sizing, total system cost (TSC) minimization of the system, reduction in battery charging cost, and determining the 24-hour load estimation and allocations of the DERs are estimated while considering the minimum SOC. The reliability constraint on battery charging from RES from 12:00 noon to 6:00 noon is applied to meet the load demand.

(iii) To address the issue of sizing and costs, the performance of a grid-connected MG system is examined and compared using the Ensemble Learning technique-based Random Forest (RF), meta-heuristic technique based on Particle Swarm Optimization (PSO), and Artificial Neural Network (ANN) for different seasons of the year for three different cases.

The rest of the paper is structured as follows: A description of the mathematical modeling of the MG system using DERs is given in Section 2. Section 3 presents the problem formulation, operational strategy, constraints for cost optimization, and reliability criteria chosen for the evaluation. The description of the computational technique is in Section 4. In Section 5, the comparison and analysis of the outcomes from various methodologies are presented. The work's conclusion is covered in the final section, Section 6.

2 System Modeling

A grid-connected microgrid with DERs is taken into consideration with the aim of identifying the best sizing and scheduling approach for efficient and reliable operation, as shown in Fig. 1. Battery energy storage systems (BESS) are used in conjunction with DERs such as RES-like solar PV systems, wind turbines, fuel cells and micro gas turbines (MT) [35]-[37]. To enable the effective and successful operation of the MG system, this part describes the mathematical modeling of various DERs.

2.1 Distributed Energy Sources (DERs)

Distributed energy resources (DERs) are a broad range of decentralized small-scale energy technologies that generate, store, and manage energy locally, rather than relying solely on centralized power plants and transmission grids [38]-[41]. The modeling of various DERs is covered below.

2.1.1 Renewable Energy Sources (RES)

RESs are emerging as major alternatives to traditional sources due to advancements like increased efficiency, improved techniques of reducing the uncertainty of energy supplies, government subsidies, etc. [42]-[44]. The mathematical modeling of RES like solar photovoltaic is explained as:

(a) Solar PV System

The solar panel instantaneously transforms solar energy from the sun into usable electrical energy. A PV cell is used to convert solar energy into electrical energy, similar to a diode with a p-n junction. Figure 2 depicts a possible equivalent circuit for a photovoltaic cell. Equation 1 shows the connection between the voltage at the output terminal and the electrical current flowing across the cells [45]-[47].

$$I_{pv}(t) = I_D + I_R + I$$

$$I_{avg,PV}(t) = I_{pv}(t) - I_{rs}\left[\exp\left(\frac{V_{pv}(t)+R_S I}{V_0 \lambda}\right)-1\right] - \frac{V_{pv}(t)+R_S I}{R} \quad (1)$$

and $V_o = \frac{kT}{q}$

The photocurrent and reverse saturation current are influenced by temperature and sun radiation in the following ways:

$$I_{rs}(t) = I_{ors}\left(\frac{T}{T_{o,NOC}}\right)^3 \exp\left(\frac{qE_g(1/T_{o,NOC} - 1/T)}{kT(t)}\right) \quad (2)$$

$$I_{PV}(t) = I_{sc}\left(1+(T-T_{o,NOC})*\lambda/1000\right)$$

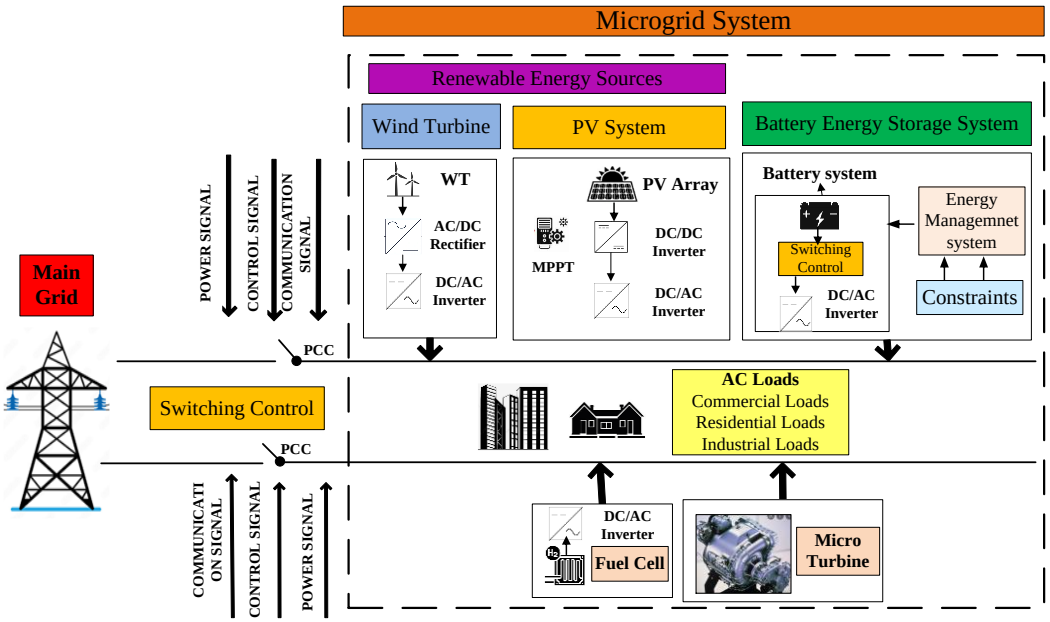

Fig.1 Systematic layout of microgrid system.

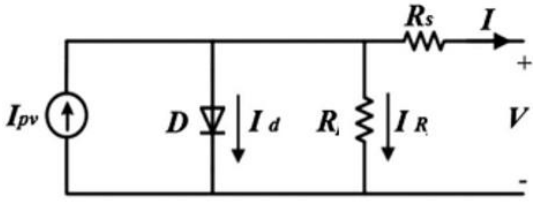

Fig. 2 Equivalent circuit of PV array.

The average voltage and current for several PV array module connections are given by:

$$I_{PV(t),avg} = n_P I_{pv} - n_P I_{or}\left[\exp\left(\frac{V_{pv(t)}+R_S I}{n_s V_0 \lambda}\right)-1\right] - n_P\left(\frac{V_{pv(t)}+R_S I}{R}\right) \quad (3)$$

where n_P is the quantity of parallel connected cells in modules, and n_s is the quantity of series connected cells within each module. The following equation combines all significant factors that affect PV production, including temperature and solar irradiation. The power production of a solar PV cell is estimated using real-time weather data for a 24-hour period for Bengaluru, Karnataka, India as;

$$P_{PV}(t) = P^{nom}_{pv,STC}(t) \times \frac{S(t)}{S_{STC}(t)}\left[1+\alpha_t\left(\left(\frac{T_a + S(t)\times}{\frac{T_{o,NOC}}{800} - 0.025}\right) - T_{o,STC}\right)\right] \quad (4)$$

$$T_{o,NOC} = T_a + \left(T_{o,NOC} - T_{a,NOC}\right)\left(\frac{S(t)}{S_{STC}(t)}\right) \times \left(1 - \frac{\Gamma_{MPPT}}{0.9}\right) \quad (5)$$

$$P_{PV}(t) = V_{PV}(t) * I_{PV,avg}(t) \quad (6)$$

where $V_{pv}(t)$ is the PV module's output voltage. To evaluate the PV performance under the various operational situations, five criteria based on α, β, γ, R_s and Γ_{MPPT} that describe the non-linear impact of the environmental variables are also taken into consideration [48]-[49]. The output power estimated will be given as:

$$P_{module}(t) = \frac{\frac{V_O}{nkT/q} - \ln\left(\frac{V_O}{nkT/q} + 0.72\right)}{1+\frac{V_O}{nkT/q}} * \left(1 - \frac{R_s}{V_O / I_{SC}}\right) * I_{sco}\left(\frac{S(t)}{S_{STC}(t)}\right)^{\alpha} * \frac{V_{OCO}}{1+\beta \ln S_{STC}(t)/S(t)} * \left(\frac{T_o}{T}\right)^{\gamma} \quad (7)$$

where α is the dimensionless coefficient associated with the particular PV module technology, β is the factor producing all of the nonlinear effects, and γ is the factor on which the photocurrent depends. PV modules must be linked in both series and parallel, depending on the voltage and current demands of the system. The power generated from the PV system can be obtained from:

$$P_{PV}(t) = n_p * n_s * P_{module}(t) * \Gamma_{MPPT} * \Gamma_{other} \quad (8)$$

(b) Wind Turbine System (WT)

The wind turbine system in a microgrid typically consists of one or more wind turbines that are connected to a power control system [50]. The swept blade area θ_A, air

density factor ϕ_a, wind speed υ, and coefficient of power δ_p, all affect the ability of wind turbines to produce electric power. The ratio can be used to express the turbine's efficiency λ ($\lambda = r\omega_T / \upsilon$) where ω_T is the speed angle of the shaft and r is the radius of the blades [51]- [52] as:

$$\delta_{P(\lambda,\alpha)} = \frac{1}{2}\left(\frac{r\delta_f}{\lambda} - 0.022\alpha - 2\right)e^{-0.255\frac{r\delta_f}{\theta_A}} \quad (9)$$

where δ_f is a blade design parameter. The wind turbine's power output is estimated as follows:

$$P_{WT}(t) = \frac{1}{2}\delta_{P(\lambda,\beta)}\phi_a\theta_A\upsilon^3(t) \quad (10)$$

This power, however, is limited to a particular range of wind speeds [53]-[54]. The correlation between the wind speed at the intended hub height is described by the following equation since wind speed changes with height:

$$\upsilon_H(t) = \upsilon_{ref}(t)\left(\frac{\upsilon_{HWT}}{\upsilon_{ref}}\right)^{\alpha_{WT}} \quad (11)$$

where $\upsilon_H(t)$ represents the wind speed at height υ_{HWT}, $\upsilon_{ref}(t)$ represents the wind speed at the reference height υ_{ref}, and α_{WT} represents the coefficient of friction. For low surface roughness and a well-exposed site, the friction coefficient α_{WT} is 1/7 [55]-[56]. Two regions make up the wind turbine's operational area: The operation area of the wind turbine can be divided into two regions:

i) In the case of a full load, over the rated wind speed υ_{rated}.

ii) Wind speed below optimum (partial load). When the load is less than the rated power $P_W^r(t)$ [57]-[58], the turbine operates with a variable rotor speed and a fixed blade pitch angle. On the other hand, the wind turbine's activity is halted at wind speeds below υ_{cutin} and a maximum υ_{rated}. The magnitude of the rated wind speed υ_{rated} and the cutoff wind speed υ_{cutoff} should be equal. The relationship between a wind turbine's power production and wind speed can be expressed as:

$$P_{WT}(t) = \begin{cases} 0 & if\ \upsilon < \upsilon_{cutin} \\ \frac{1}{2}\delta_{P(\lambda,\beta)}\phi_a\theta_A\upsilon^3(t) & \upsilon_{cutin} \le \upsilon \le \upsilon_{rated} \\ P^r_{W(t)} & if\ \upsilon_{rated} \le \upsilon \le \upsilon_{cutoff} \\ 0 & if\ \upsilon > \upsilon_{cutoff} \end{cases} \quad (12)$$

2.1.2 Fuel Cell (FC)

An electrochemical device known as a Fuel Cell (FC) transforms chemical energy into electrical energy while also producing heat and water as waste products [59]-[60]. The modeling of FC includes the total power of the fuel cell stack is P_{FC} as well as average voltage of each cell in the stack is V_{FC} for n no of cells. If V_{FC} is not mentioned, it can be assumed in the range 0.6 and 0.7 V, as most fuel cells function in this region. If the efficiency is given, then V_{FC} can be calculated using Equation 4. If no figures are provided, then using V_{FC} = 0.65 V will give a good approximation and result. If the fuel cell is pressurized, the estimate should be slightly higher [61]-[62]. The power will be computed as follows if the voltage of each cell in the stack is V_{FC} shown in Equation 13:

$$V_{FC,avg}(t) = \upsilon_o - \upsilon_{ac} - \upsilon_{ohm} - \upsilon_{con} \quad (13)$$

$$\Gamma_{FC} = \frac{P_{FC}(t)}{P_H(t)}$$
$$P_{FC}(t) = V_{FC,avg}(t) \times I_{FC}(t) \times n \quad (14)$$
$$So,\ I_{FC}(t) = \frac{P_{FC}(t)}{V_{FC,avg}(t) \times n}$$

when there is no current flowing, referred to as the "open-circuit" voltage. The cell produces a reversible voltage, υ_o, as shown in [63]-[64]:

$$P_H(t) = \upsilon_o I_{FC}(t)$$
$$and\ \upsilon_o = \frac{\Delta G}{n_e F} \quad (15)$$

2.1.3 Micro Gas Turbine (MT)

A micro gas turbine (MGT) is a small-scale power generation system that uses combustion to produce electricity. It is a promising technology for Microgrid applications, as it offers several advantages over other conventional power generation methods such as internal combustion engines or gas turbines. MGTs can be used in various kinds of Microgrid applications, including settings for homes, businesses, and industries [65]-[67].

The compressor, combustor, turbine, and electric generator are the various components of a small gas turbine. Similar to diesel generators, microturbines are subject to minimum and maximum power rating constraints. A small, high-speed gas turbine called the MT typically produces power between 20 kW and 500 kW. The two primary types of MTs are single-shaft and split-shaft, with the former having the generator and turbine on the same shaft.

2.1.4 Battery Energy Storage System (BESS)

In a Microgrid system, BESS can provide a regulating reserve, a kind of auxiliary service, to decrease frequency deviations brought on by rapid changes in renewable energy by altering active power for frequency control [68]-[70]. The design of the battery, backup time, lifespan of the battery, battery temperature, depth of discharge, necessary reserve power, and renewable energy sources are some of the factors that affect the ESS rating. The maximum capacity of the battery system is often calculated using the state of charge (SOC) using:

$$\frac{SOC(t)}{SOC(t-1)} = \int_{T-1}^{T} \frac{P_B(t)\Gamma_{batt}}{\upsilon_{BUS}} dt \quad (16)$$

$SOC(t)$: State of charge at time 't'.

$SOC(t-1)$: State of charge at time '(t-1)'.

A positive value for $P_B(t)$ indicates that the battery is charging and a negative value indicates that it is draining. The battery's round-trip efficiency in this particular case is determined as follows:

$$\eta_{Batt} = \sqrt{\eta_{Batt}^{c}\eta_{Batt}^{d}} \quad (17)$$

The total capacity of the battery estimated considering the SOC is:

$$\psi_n(Ah) = \frac{n_{Battery}}{n_{Battery}^{s}}\psi_b(Ah) \quad (18)$$

where $\psi_b^1(Ah)$ is the battery capacity of a single battery, the number of total batteries is $n_{Battery}$ and $n_{Battery}^{s}$ is the batteries connected in series. There is a minimum discharge limit known as $SOC_{\min}$ that the battery bank cannot go over. The formula, which can be used to compute the batteries connected in series is,

$$n_{Battery}^{s} = \frac{\upsilon_{BUS}}{\upsilon_{Battery}} \quad (19)$$

where is a single battery's voltage $\upsilon_{Battery}$. Now, the battery power can be calculated as:

$$P_B^{\max} = \frac{n_{Battery}\upsilon_{Battery}I_{\max}}{1000} \quad (20)$$

where $I_{\max}$ is the maximum charging current of the battery in amperes. The combined power generated by the WTs and PVs at hour t is estimated as follows:

$$P_G(t) = P_{PV}(t) + P_{WT}(t) \quad (21)$$

It is possible that the total power produced won't be sufficient to supply all of the electricity required. In such a system, the battery's SOC is calculated using the equation shown below. When the load during the charging process exceeds the combined output of the WT and PV units, the useful battery capacity at time t is determined by:

$$SOC(t) = SOC(t-1)*(1-\sigma_{self}) + \left(\Theta_g^t(t) - \frac{P_D(t)}{\Gamma_{inv}}\right)\Gamma_{ch} \quad (22)$$

since the maximum energy held in the storage system cannot be greater than the maximum state of charge $SOC_{\max}$. The following constraint must be adhered to during optimization:

$$SOC_{\min}(t) \le SOC(t) \le SOC_{\max}(t) \quad (23)$$

when the load exceeds the generation, the battery starts discharged (more energy can be supplied from the battery) [71]-[72]. Therefore, it is possible to calculate the battery capacity that is accessible at hour t by:

$$SOC(t) = SOC(t-1)*(1-\sigma_{self}) + \left(\frac{P_D(t)}{\Gamma_{inv}} - \Theta_g(t)\right)/\Gamma_{dch} \quad (24)$$

The following constraint is in effect while discharging

$$SOC(t) \ge SOC_{\min}(t) \quad (25)$$

The charging or discharging situation is the only mode that BESS can operate in simultaneously. The charging of batteries in this research is considered from RES only from 12:00 PM to 6:00 PM during off-peak hours. The battery's capacity to charge and discharge is determined as follows:

Charging Mode:

$$E_{ch}(t) = \left(\frac{P_{WT}(t)+P_{FC}(t)+P_{MT}(t)+P_G(t)+P_{PV}(t)}{\Gamma_{Conv}} - P_D(t)\right) * \Delta t * \Gamma_{ch} \quad for\ t = 12\ to 18\ hours \quad (26)$$

$$SOC(t) = SOC(t-1)(1-\sigma) + E_{ch}(t)\ , charge\ from\ grid$$

Discharging Mode

$$E_{dch}(t) = \left(P_D(t) - \frac{P_G(t)+P_{WT}(t)+P_{FC}(t)+P_{MT}(t)+P_{PV}(t)}{\Gamma_{Conv}}\right) * \Delta t * \Gamma_{dch} \quad (27)$$

$$SOC(t) = SOC(t-1)(1-\sigma) - E_{dch}(t)$$

$$SOC(t) = SOC(t-1) + \Delta t\left(\frac{\Gamma_{ch}P_{B,t}^{ch}}{E_m} - \frac{E_m}{\Gamma_{dch}P_{B,t}^{dch}}\right) \quad (28)$$

2.1.5 Modeling of Thermal Unit

The startup cost and operating cost are the two components of the thermal power generator. A quadratic function of the power is frequently used to express an operation's cost:

$$f\left(P_{G_i}(t)\right) = \sum_{i=1}^{N}\left(\left(a_i P_{G_i}^2(t) + b_i P_{G_i}(t) + c_i\right)\right) \quad (29)$$

$$SUC(t) = SUC_{G_i}\left(u_{G_i}(t) - u_{G_i}(t-1)\right)$$

2.1.6 Power Converter

A power converter is necessary if a system has both AC and DC components. The output from solar PV and batteries is DC even though the load is believed to be AC. The peak power demand $P_P(t)$ determines the converter's size. The calculation for the inverter rating $P_{inv}(t)$ is represented in equation 31 [90].

$$P_{inv}(t) = \frac{P_P(t)}{\Gamma_{inv}} \quad (30)$$

3 RANDOM FOREST TECHNIQUE

The Random Forest technique is a powerful and widely used machine learning algorithm that belongs to the ensemble learning family. It is particularly effective in both classification and regression tasks and has gained popularity due to its ability to provide accurate predictions and handle complex datasets. Random Forest is based on the concept of decision trees, which are tree-like models that make predictions by partitioning the input space into regions and assigning a class or value to each region. However, decision trees tend to suffer from overfitting, which means they can become overly complex and have poor generalization performance [73]-[74]. To overcome this limitation, Random Forest combines the predictions of multiple decision trees to make more robust and accurate predictions.

Instead of relying on a single decision tree, it creates an ensemble of decision trees, where each tree is trained on a different subset of the training data and features. The key idea behind Random Forest is that by introducing randomness in the learning process, the ensemble of trees can collectively reduce overfitting and improve generalization performance. Randomness is introduced in

two ways: random sampling of the training data and random feature selection. During the training process, each tree is trained on a bootstrap sample of the original training data, which means that some instances may be repeated and others may be left out. This sampling technique is known as bagging. Furthermore, at each node of a decision tree, Random Forest only considers a random subset of features for splitting, rather than using all available features. This feature subsampling is known as the random subspace method or feature bagging. By doing so, Random Forest decorrelates the decision trees, reducing their tendency to make similar predictions and increasing the diversity within the ensemble [75]-[77]. To make predictions, Random Forest aggregates the predictions of all the individual trees. In classification tasks, it uses majority voting, where the class with the most votes among the trees is selected as the final prediction. In regression tasks, it takes the average or the median of the predicted values from all the trees.

The mean squared residual at the node is a common splitting criterion in the context of regression if the response values at the node are $y_1, y_2 ..... y_n$.

$$Q = \frac{1}{n}\sum_{i=1}^{n}(y_i - \bar{y})^2 \tag{31}$$

where n_t is the number of elements at the node and

$$\bar{y} = \frac{1}{n}\sum_{i=1}^{n} y_i \tag{32}$$

is the estimated value of each node object. A common splitting criterion $1,..k$ in the context of classification, where K classes are denoted, is the Gini index.

$$Q = \sum_{K=K'}^{K} \hat{p}_K \hat{p}_{K'} \tag{33}$$

where $\hat{p}_K$ is the proportion of observations of class k in the node. The splitting criteria provide a measurement of a node's "goodness of fit" (in regression) or "purity" (in classification), with large values signifying a node that is neither pure nor well-fitted. Two descendant nodes are produced by a candidate split, one on the left and one on the right. The split is chosen to reduce: As indicated by the splitting criterion for the two potential descendants as Q_L and Q_R, and the corresponding size of the sample as n_L and n_R,

$$Q_{\text{split}} = n_L Q_L + n_R Q_R . \tag{34}$$

Finding the appropriate split for a continuous predictor variable requires sorting the predictor's values and taking into account splits between each unique pair of successive values. The interval's midpoint is typically used, but any value within the range will do. For a predictor variable, the values of, Q_L, Q_R and consequently Q_{split} are computed for all potential combinations of selecting a subset of categories to proceed to each descendant node [78]. The Random Forest Decision Tree Regression uses a real-time data set of six months from Bengaluru, Karnataka, India as shown in Fig. 3. The following procedure is used for creating the Random Forest model.

Procedure for Random Forest Model

Initial Stage

Step 1: The dataset variables are divided into training data and testing data.

Step 2: the Training dataset T_1, T_2….T_N is divided into N size Bootstrap samples S_1, S_2, ….S_N.

(Randomly select a bootstrap sample from the original training data. This means randomly selecting instances with replacements, allowing some instances to appear multiple times and others to be left out).

Construction Stage

Step 3: Initialize the number of trees in the forest and other hyperparameters such as the number of decision trees D_1, D_2…. D_N., no. of node size, etc.

Here, Number of Trees = 100

Number of variables in each split = 3

Minimum Node size = 4

(a. Build a decision tree using the selected bootstrap sample and features. The tree is constructed by recursively splitting the data based on feature thresholds that maximize the information gain or other impurity measures.

b. Continue splitting until a stopping criterion is met, such as reaching the maximum depth or minimum number of instances in a leaf node).

Final Outcome

Step 4: Once all trees are built, the Random Forest model is used for output.

a. For classification tasks: Each tree in the forest predicts the class label of a given instance. The final predicted class is determined by majority voting among all the trees.

b. For regression tasks: Each tree predicts a continuous value for a given instance. The final predicted value is typically the average or the median of all the tree predictions.

$$\hat{f}(x) = \frac{1}{N}\sum_{i=1}^{N}\hat{C}_i(x) \quad for\ regression \tag{35}$$

The Random Forest algorithm also allows for additional functionalities, such as measuring feature importance. Feature importance can be calculated based on how much each feature contributes to reducing the impurity or error in the decision trees.

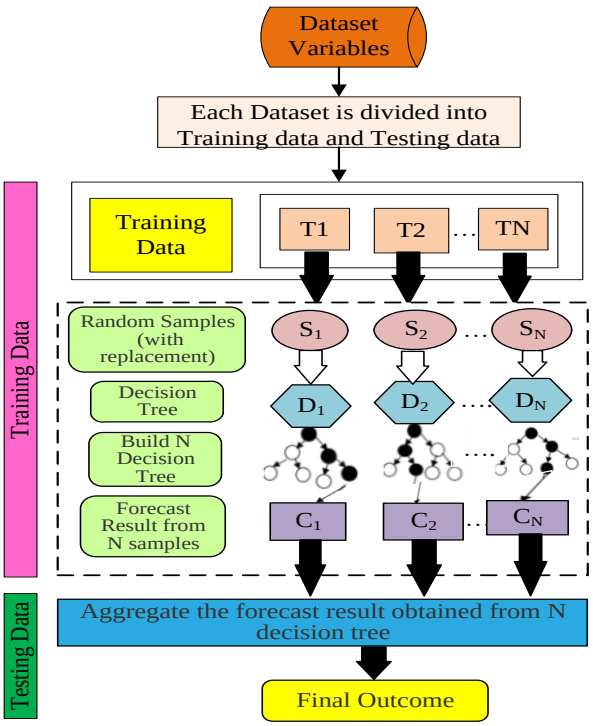

Fig.3 Layout of Random Forest Model.

4 Formulation of Problem

4.1 Objective Function

The main objective of this research is to investigate and evaluate (i) the MG system's Total System Cost (TSC). (ii) to achieve the optimum battery size (iii) to lower the cost of battery charging. The proposed challenge is presented as a multi-objective optimization problem. The objective function is comprised of the costs of the following items: (i) the cost of the solar PV system, WT, FC, MT, and BESS; (ii) the cost of operation and maintenance; (iii) the cost of generation; and (iv) the cost of buying and reselling power from/to the grid. This section exemplifies the objective function and its associated constraints.

$$Min\ TSC(X)=\sum_{t=1}^{NT}\begin{pmatrix} C_{PV}^{t}+C_{WT}^{t}+ \\ TC_{MT}^{t}+TC_{FC}^{t} \\ +C_{G}^{t}+C_{BESS}^{t}+C_{OM}^{t} \end{pmatrix}+\sum_{t=1}^{NT}\left(C_{Buy}^{t}-C_{Sell}^{t}\right) \quad (36)$$

The operational costs for the solar panel array and the wind turbine are computed as

$$C_{PV}^{t}=\Im^{PV}P_{PV}(t)$$
$$C_{WT}^{t}=\Im^{WT}P_{WT}(t) \quad (37)$$

Microturbine (MT) running costs also include their startup costs (SUC) is given as

$$C_{MT}^{t}=\left(\frac{C_{ng}}{\partial}\right)\sum\frac{P_{MT}(t)}{\Gamma_{MT}(t)}$$
$$SUC_{MT,t}=Start_{MT}*\max(0,u_{MT,t}-u_{MT,t-1}) \quad (38)$$
$$TC_{MT}^{T}=C_{MT}^{t}+SUC_{MT,t}$$

Fuel Cell (FC) and Micro Turbine (MT) running costs are computed as:

$$C_{FC}^{t}=\left(\frac{C_{ng}}{\partial}\right)\sum\frac{P_{FC}(t)}{\eta_{FC}(t)}$$
$$SUC_{FC,t}=Start_{FC}*\max(0,u_{FC,t}-u_{FC,t-1}) \quad (39)$$
$$TC_{FC}^{t}=C_{FC}^{t}+SUC_{FC,t}$$

Start-up and running expenses are the two elements of the thermal power generator. A quadratic function of the power is frequently used to express an operation's cost is expressed as:

$$C_{G}^{t}=C_{f}\sum_{i=1}^{N}\begin{pmatrix}\left(a_{i}P_{G_i}^{2}(t)+b_{i}P_{G_i}(t)+c_{i}\right) \\ +SUC_{G_i}\left(u_{G_i}(t)-u_{G_i}(t-1)\right)\end{pmatrix} \quad (40)$$

The constant repair and maintenance costs of dispatchable and non-dispatchable units are:

$$C_{OM}^{t}=OM_{MT}^{t}+OM_{FC}^{t}+OM_{PV}^{t}+OM_{WT}^{t}+OM_{G}^{t} \quad (41)$$

The operational costs of the BESS and utility, the fuel and OM costs of DERs, the start-up costs of MT and FC, as well as the daily cumulative cost of batteries, make up the total charges for the MG. The price of batteries includes both the initial, fixed cost (FC) and continual maintenance and repair (MC) costs.

The cost of installed batteries may be calculated using the formula below.

$$C_{B}^{t}=\frac{C_{B,\max}}{365}\left(\frac{IR(1+IR)^{LT}}{(1+IR)^{LT}-1}FC_{B,t}+MC_{B,t}\right) \quad (42)$$

The following equations represent the functions of power purchase cost and power selling revenue:

$$C_{Buy}^{t}=c_{Buy}(t)P_{Buy,t}\Delta t$$
$$C_{sell}^{t}=c_{Sell}(t)P_{Sell,t}\Delta t \quad (43)$$

4.2 Formulation of Constraints

Grid Constraints: The supply of the main grid must be provided within the given limits.

$$P_{Grid,\min}(t)\le P_{Grid}(t)\le P_{Grid,\max}(t),\ t=1.....24 \quad (44)$$

Dispatchable DGs constraints: It regulates the various DGs' maximum power output limits; they must provide power within those limits.

$$P_{MT,\min}(t)\le P_{MT}(t)\le P_{MT,\max}(t)\ ,t=1...24$$
$$P_{FC,\min}(t)\le P_{FC}(t)\le P_{FC,\max}(t)\ ,t=1...24 \quad (45)$$

Power exchange constraints: Operation constraints for power exchange between the microgrid and the main grid. The limits of power purchasing from/selling to the main grid are-

$$0\le P_{Buy}(t)\le \overline{P}_{Buy}(t)u_{Buy}(t)$$
$$0\le P_{Sell}(t)\le \overline{P}_{Sell}(t)u_{Sell}(t) \quad (46)$$

Operating Reserve (OR) Constraints: In MG systems, reliability is achieved by acquiring the energy storage, e.g. BESS and operating reserve. In each time step, operating reserve (OR) is the addition of stand-by generation capacity of turned-on BESS, FC, MT, and Grid. It can be supplied to the MG in less than 10 minutes and defined by

$$P_{G}(t)+P_{MT}(t)+P_{FC}(t)+P_{PV}(t)$$
$$+P_{WT}(t)+P_{B}(t)=P_{D}(t)+R_{operating}(t) \quad (47)$$
$$where\ t=1,.....24$$

BESS Constraints: It provides the maximum and minimum charging and discharging rate of BESS

Discharging mode

$$C_{B,t+1}=\max\left\{\left(C_{B,t}-\frac{\Delta t\,P_{B}(t)}{\Gamma_{dch}}\right),C_{B,\min}\right\},\ t=1.....24 \quad (48)$$
$$P_{B}^{dch}(t)\le P_{B}(t)\le P_{B}^{ch}(t),\ t=1.....24$$

Charging Mode

During peak hours from 12 P.M. to 6 P.M. Battery will get charged from RESs to minimize cost.

$$C_{B,t} = \min\left\{\left(C_{B,t} - \Delta t\, P_B(t)\Gamma_{ch}\right), C_{B,\max}\right\}, \quad t = 1.....11 \& t = 19....24 \; off\ peak\ hours$$
$$C_{B,t+1} = \min\left\{\left(C_{B,t} - \Delta t\, P_B(t)\Gamma_{ch}\right), C_{B,\max}\right\}, \quad t = 12.....18 \; charge\ from\ RESs \tag{49}$$

The battery constraints must be

$$P_B^{dch}(t) \le P_B(t) \le P_B^{ch}(t),\ t = 12.....18 \tag{50}$$

The battery State of charge (SOC) constraints.

$$SOC_{\min}(t) \le SOC(t) \le SOC_{\max}(t)$$

where

$$SOC(t) = SOC(t-1) + \Delta t\left(\frac{\Gamma_{ch} P_B^{ch}(t)}{E_m} - \frac{P_B^{dch}(t)}{\Gamma_{dch} E_m}\right) \tag{51}$$

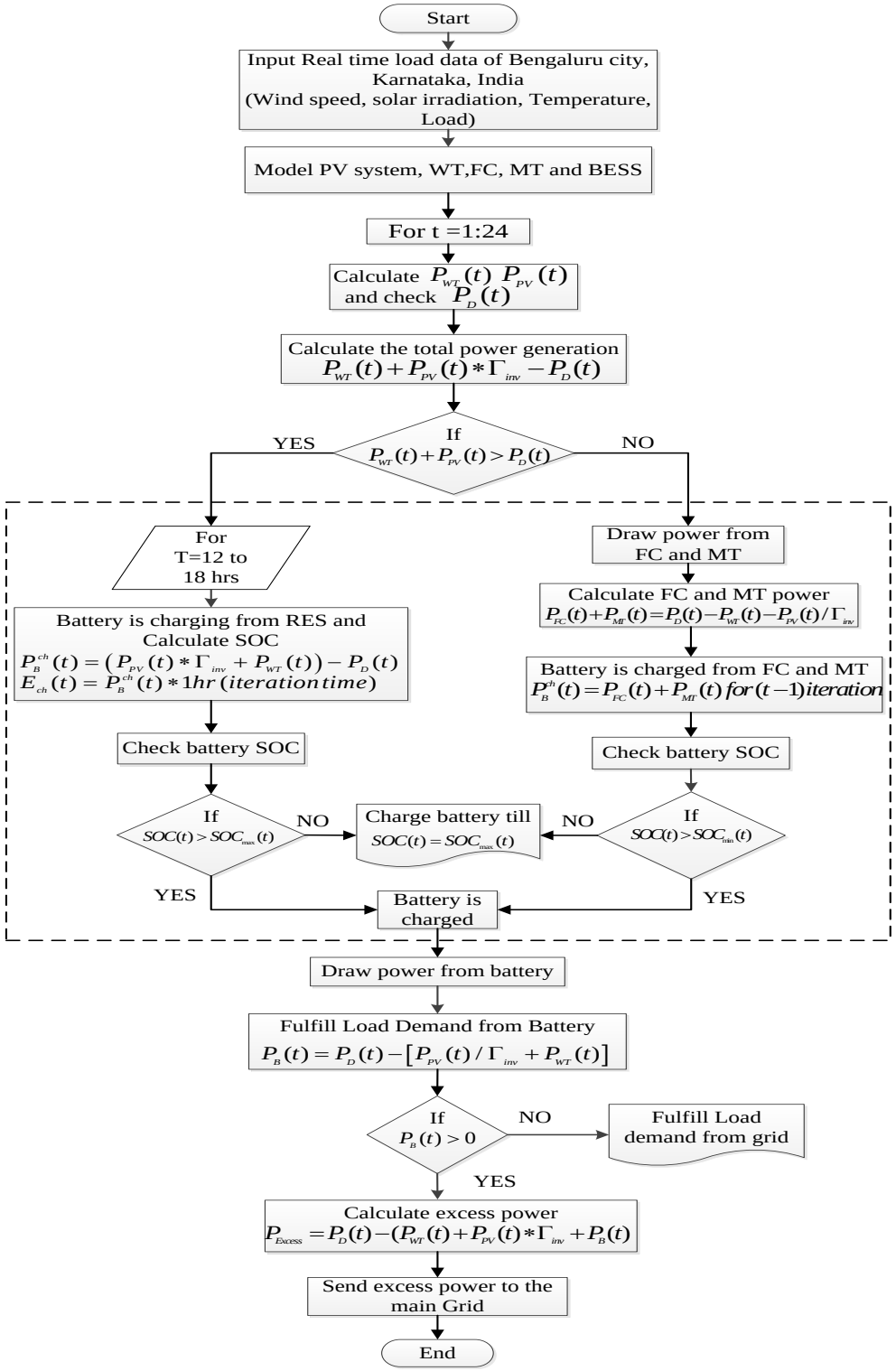

Fig. 4 Operational strategy and battery charging process of grid-connected MG system with DERs.

4.3 Formulation of Operational Strategy

The hybrid energy system must have effective power management to guarantee system dependability. This system changes to running FC and MT, which are put on the lowest priority list when solar, wind, and batteries are not enough to match the load demand. In order to fulfill the above criteria, the steps of an operational strategy are as follows:

Operational Strategy 1:

A. At first, if the combined production of solar PV panels and wind turbines is sufficient and load demand is low, then, renewable energy sources can meet demand on their own and charge the batteries from 12:00 PM to 6:00 PM during off-peak hours.

$$P_B^{ch}(t) = \left(P_{PV}(t) * \Gamma_{inv} + P_{WT}(t)\right) - P_D(t) \quad (52)$$
$$E_{ch}(t) = P_B^{ch}(t) * 1hr\,(iteration\,time)$$

B. The battery SOC is checked and power demand is fulfilled from batteries and RES.

$$P_B(t) = \left[P_{PV}(t) / \Gamma_{inv} + P_{WT}(t)\right] - P_D(t) \quad (53)$$

where $P_D(t)$ is the total load demand and Γ_{inv} represents the efficiency of the DC/AC converter. The generation of total power by solar PV panels $P_{PV}(t)$ is estimated as:

$$P_{PV}(t) = P_{PV,\sin gle}(t) n_{PV} \quad (54)$$

If the power generated by a single solar PV panel is $P_{PV,\sin gle}(t)$ and there are η_{pv} solar PV panels overall,

Additionally, the generation by wind turbines $P_{WT}(t)$ is expressed as:

$$P_{WT}(t) = P_{WT,\sin gle}(t) n_{WT} \quad (55)$$

where $P_{WT,\sin gle}(t)$ is the power generated by a single wind turbine and n_{WT} is the number of wind turbines.

Operational Strategy 2: If the amount of generating power produced by the wind turbines and solar PV panels is insufficient, the load demand is fulfilled from FC and MT and batteries are also charged from it. There are two applications for FC and MT, which are covered here.

A. First of all, when it is in operation, it only produces the electricity needed to fulfill the primary load demand. Calculations of the power produced by the FC and MT are as follows:

$$P_{FC}(t) + P_{MT}(t) = P_D(t) - P_{WT}(t) - P_{PV}(t) / \Gamma_{inv} \quad (56)$$

B. The batteries are also charged from FC and MT after fulfilling the load demand to minimize charging costs.

$$P_B^{ch}(t) = P_{FC}(t) + P_{MT}(t)\ for\,(t-1)\,iteration \quad (57)$$

Operational Strategy 3: When solar and wind energy are insufficient and batteries are unable to produce enough power to meet the load demand, fuel cells and micro gas turbines (MT) are used to supply electricity to the load. Secondly, if the load demand exceeds during peak hours and power generation from FC and MT is insufficient then excess power demand is fulfilled from the main grid and batteries are it runs at a minimal load ratio or rated capacity.

Operational Strategy 4: If the amount of energy $P_B(t)$ in either of the aforementioned circumstances exceeds the maximum permissible capacity $P_b^{\max}(t)$ of the battery bank, The excess power is calculated as:

$$P_{Excess} = P_D(t) - \left(P_{WT}(t) + P_{PV}(t) * \Gamma_{inv}\right) + P_B(t) \quad (58)$$

This excess power can be used for charging EVs or provided to charge the BESS during off peak hours.

Figure 4 illustrates a simplified flow chart of the proposed MG system's operating strategy and battery charging process. In this system, the FC and MT are given the lowest priority. They will only turn on when solar, wind, or batteries are unable to deliver the power to the load demand.

5 Result Analysis and Discussion

This section provides an overview of the outcomes obtained from the application of RF, PSO, and ANN approaches to the proposed grid-connected Micro Grid (MG) system shown in Fig. 1. Using the aforementioned methodologies, the optimum battery, reduction in battery charging cost and Total cost of power generation is estimated for real-time load data of Bengaluru city (Karnataka, India) [79]-[80] for various seasons. For the proposed MG system, a population size of 25 for 100 iterations is used as a comparison for different techniques in order to confirm the results. At 0.98 lagging power factor in the current work, all DGs produce active power. Batteries are charged and discharged at an equal and constant rate of 80%. The constraints of charging the battery from RESs from 12 noon to 6 noon are also adhered to for the MG system. The various configurations of MG with DERs taken into consideration for analysis include:

- Case-I: MG system with RESs (solar PV, WT) and Battery
- Case-II: MG system with FC, MT, and Battery
- Case-III: MG system with DERs (solar PV, WT, FC, MT, and Battery)

5.1.1 Case-I: MG system with RESs (solar PV, WT) and Battery

In Case 1, the total power generation from RESs and battery is optimized to meet the electrical load demand using RF, PSO, and ANN. As seen in Fig. 6(a), during the winter, RF power generation is at its best between the hours of 2 and 6 pm, exceeding load demand, whereas ANN power output is at its lowest between the hours of 6 and 8 am and 11 am and 3 pm. The overall power generation in the RF and ANN scenarios varies during the spring due to climate change, as illustrated in Fig. 6(b). Due to the hot and humid weather, there is a greater need for electricity during the summer. As a result, it becomes difficult for RF, PSO, and ANN to offer optimal generation to meet load demand, as shown in Fig. 6(c). The monsoon season's humid and rainy weather affects both the ideal generation and load demand, as can be shown

in Fig. 6(d).

The battery charging and discharging states are also evaluated and shown in Fig. 7(a)-(d) for various seasons for RF, PSO, and ANN approaches. The battery state shows that load demand is not fulfilled because of the intermittent nature of RES. Therefore, CASE II and CASE III are also analyzed to determine the performance of the Grid-Connected MG system.

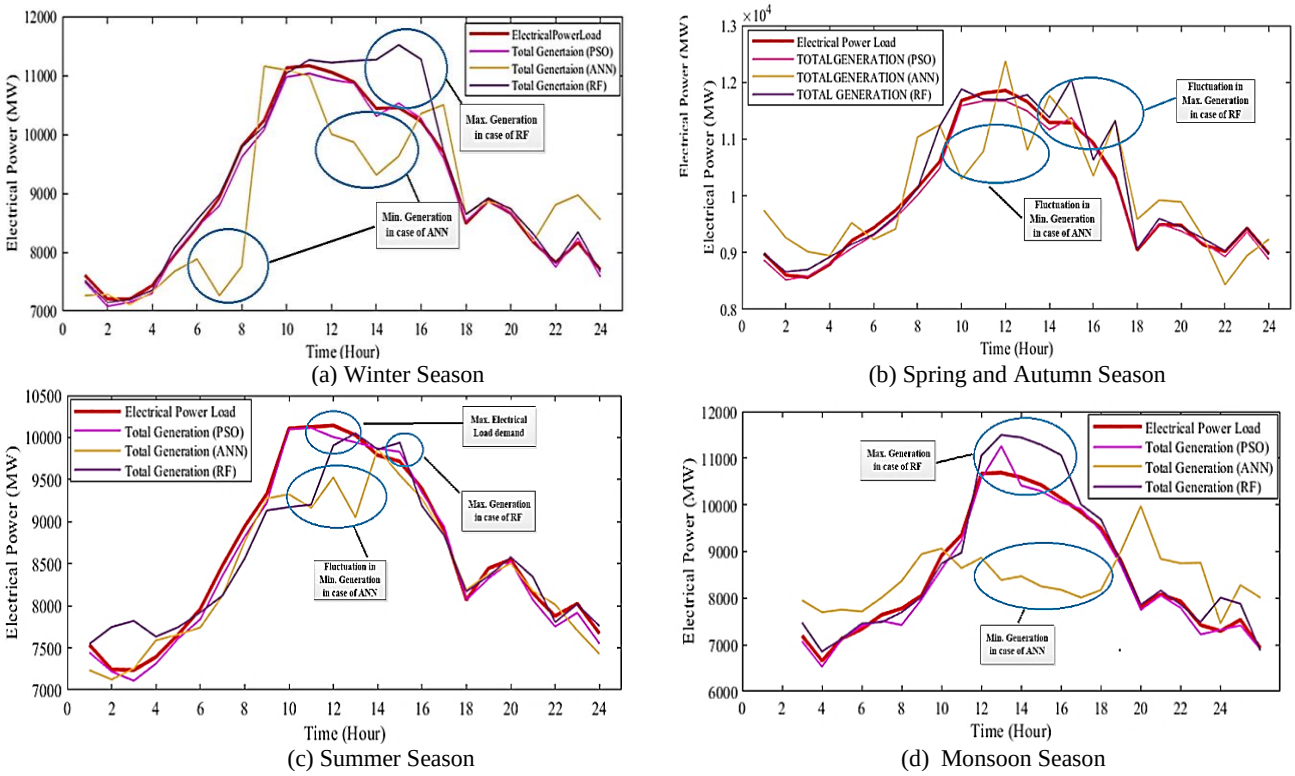

Fig. 6 Optimal total electrical power generation to meet electrical load demand for CASE 1 using RF, PSO and ANN for (a) Winter Season (b) Spring and Autumn Season (c) Summer Season (d) Monsoon Season.

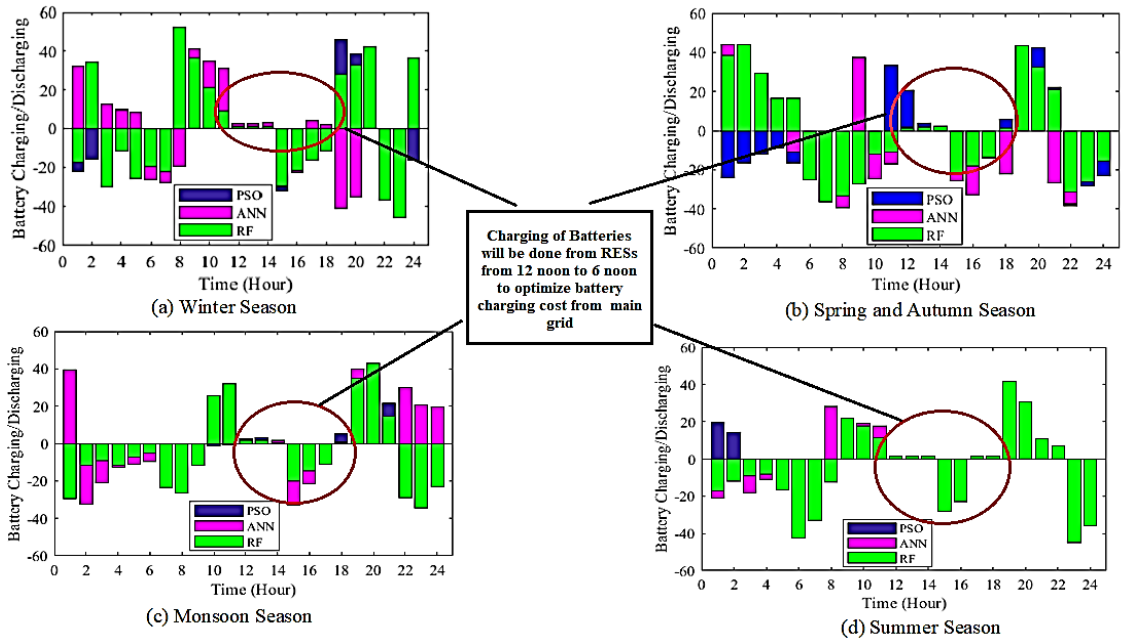

Fig. 7 Optimal battery charging and discharging state for RF, PSO, and ANN for CASE I .

5.1.2 Case-II: MG system with FC, MT, and Battery

In Case II, the study is carried out to determine the optimum cost, schedule, and sizing for the MG system with

FC and MT with batteries for various seasons. Since there is less load consumption during the winter, the optimal period to generate maximum power is between noon and 2 pm in the case of RF but in the case of ANN, there is a variation in the generation of power between 11 am and 3 pm, as illustrated in Fig. 8(a). As shown in Fig. 8(b), there is a variation and fluctuation in generation during the spring season in the case of ANN. In the summer, PSO and ANN produce the least amount of energy from 5 to 7 p.m., while ANN and RF produce the maximum energy from 10 to 12 p.m. Due to changes in load demand during monsoon season, ANN and RF's optimal generation also changed, whereas PSO provides consistent generation.

The optimal battery charging and discharging condition analysis is depicted in Fig. 9(a)-9(d). In this case, the load demand is fulfilled from the FC, MT, and batteries, and the remaining generated power is sold to the main grid or it can be used for EV charging, etc. Due to the continuous operation of the micro gas turbine to meet the load demand, the cost of power generation is higher in this particular case. The expense of operation and maintenance is also escalating.

5.1.3 Case-III: MG system with DERs (solar PV, WT, FC, MT, and Battery)

In Case III, the analysis of the proposed grid-connected MG system with all the DERs is considered. The total power generation from DERs is optimized to meet the electrical load demand using RF, PSO, and ANN as depicted in Fig.10(a)-10(d) for different seasons. RF generates the maximum power during the winter months when compared to ANN and PSO. Due to load variations, maximum and minimum generation for RF and ANN fluctuates over the seasons of spring and autumn. In the summer, RF produces the maximum energy, whereas ANN produces the least energy. Maximum and lowest generations have fluctuated during the monsoon season for RF and ANN.

The optimal battery charging and discharging conditions with constraint are also analyzed using RF, PSO, and ANN techniques for different seasons as shown in Figure 11(a)-11(d). Thus, it can be seen that the optimal results obtained from CASE III are better than CASE I and CASE II.

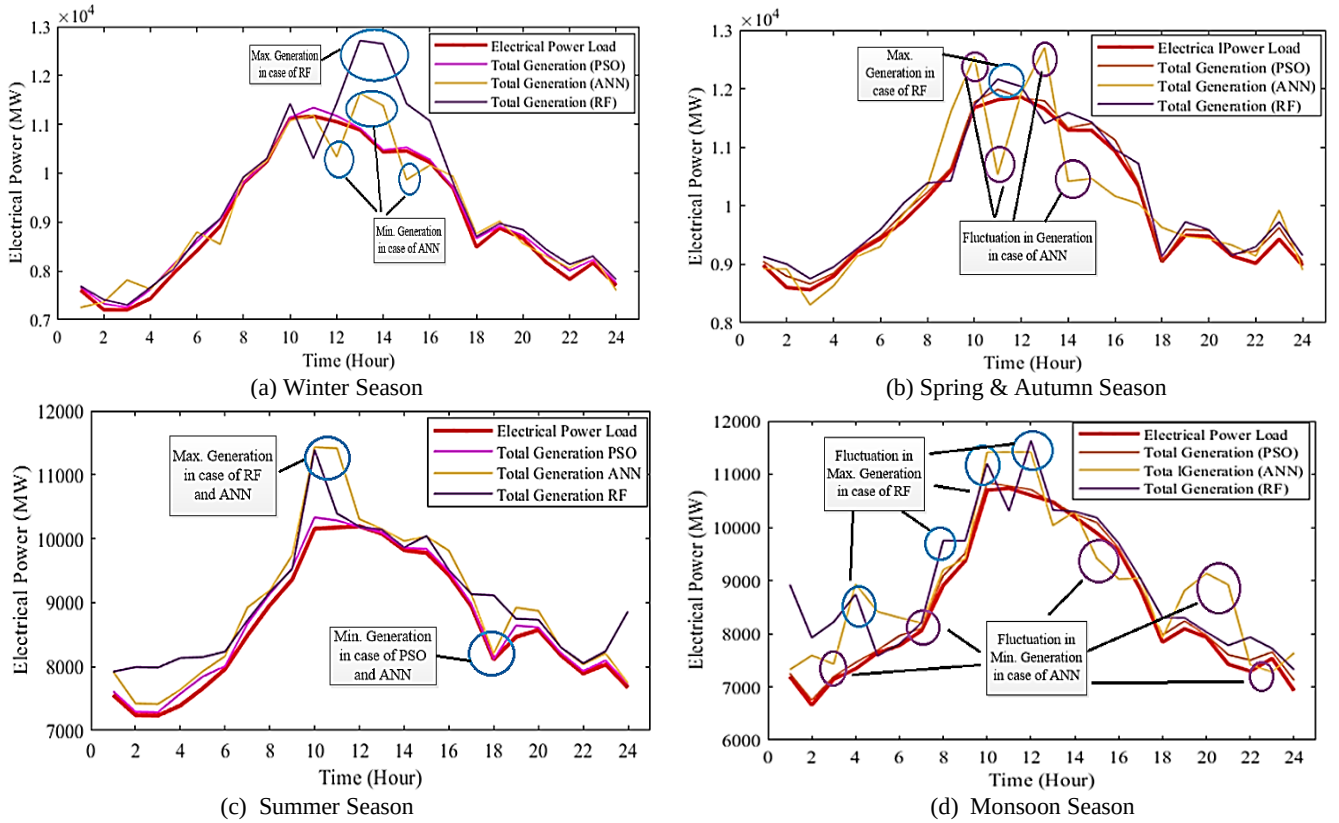

Fig. 8 Optimal total electrical power generation to meet electrical load demand for CASE II using PSO, ANN, and RF (a) Winter Season (b) Spring and Autumn Season (c) Monsoon Season (d) Summer Season.

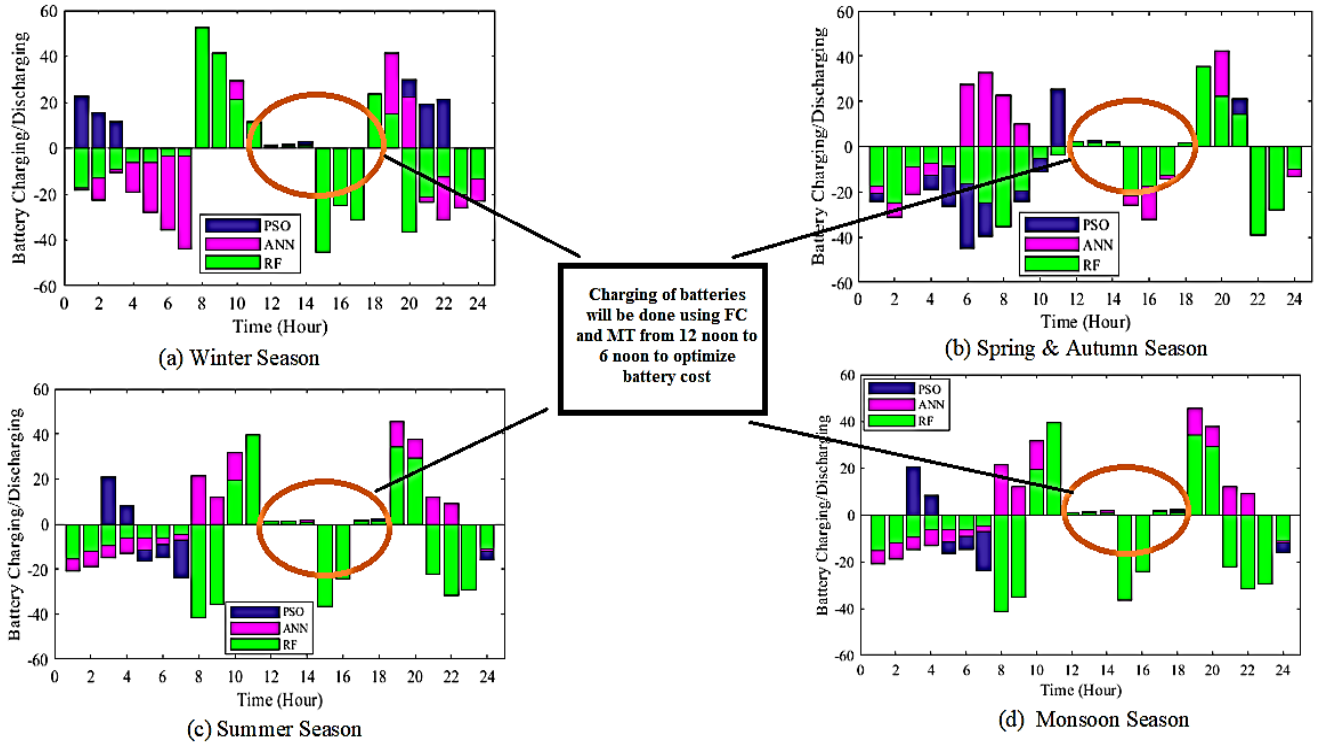

Fig. 9 Optimal battery charging and discharging state for PSO, ANN, and RF for CASE II.

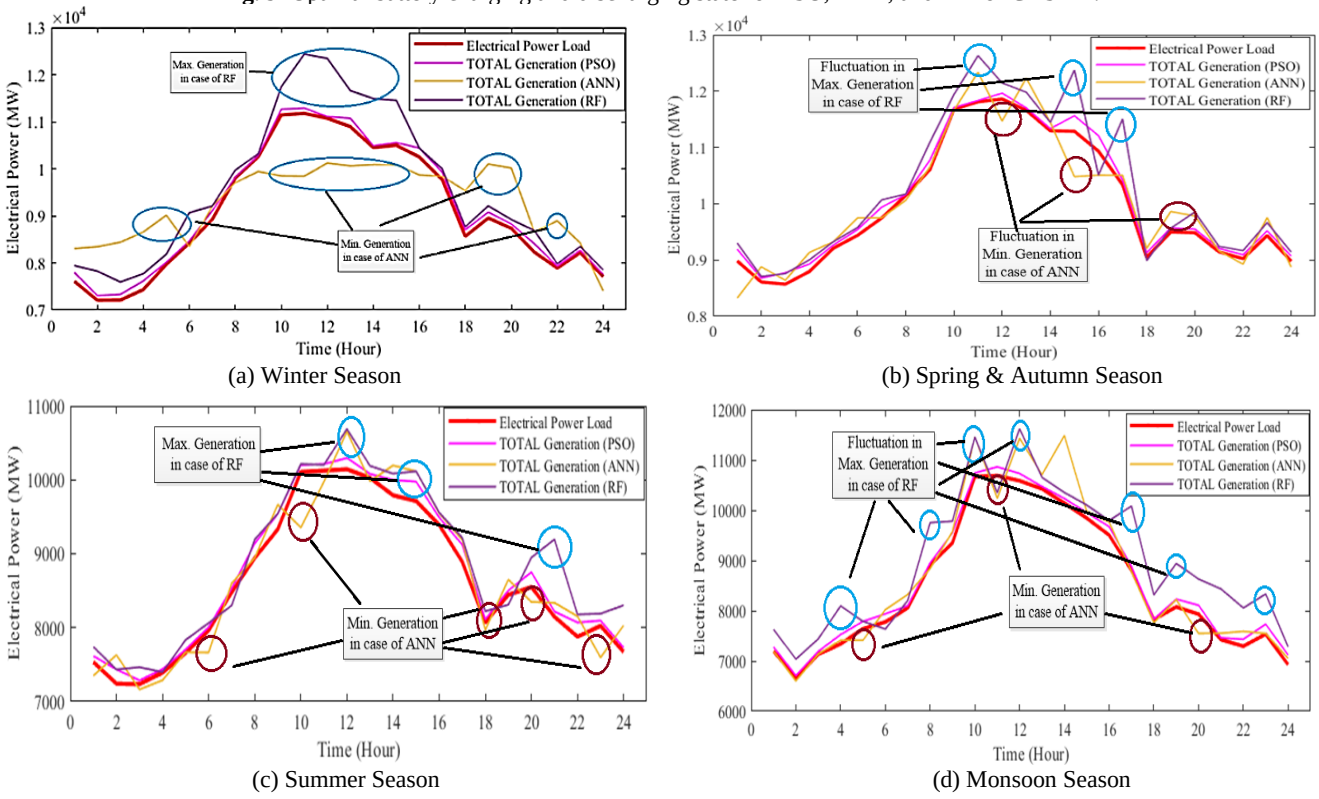

Fig. 10 Optimal total electrical power generation to meet electrical load demand for CASE III using PSO, ANN, and RF (a) Winter Season (b) Spring and Autumn Season (c) Monsoon Season (d) Summer Season.

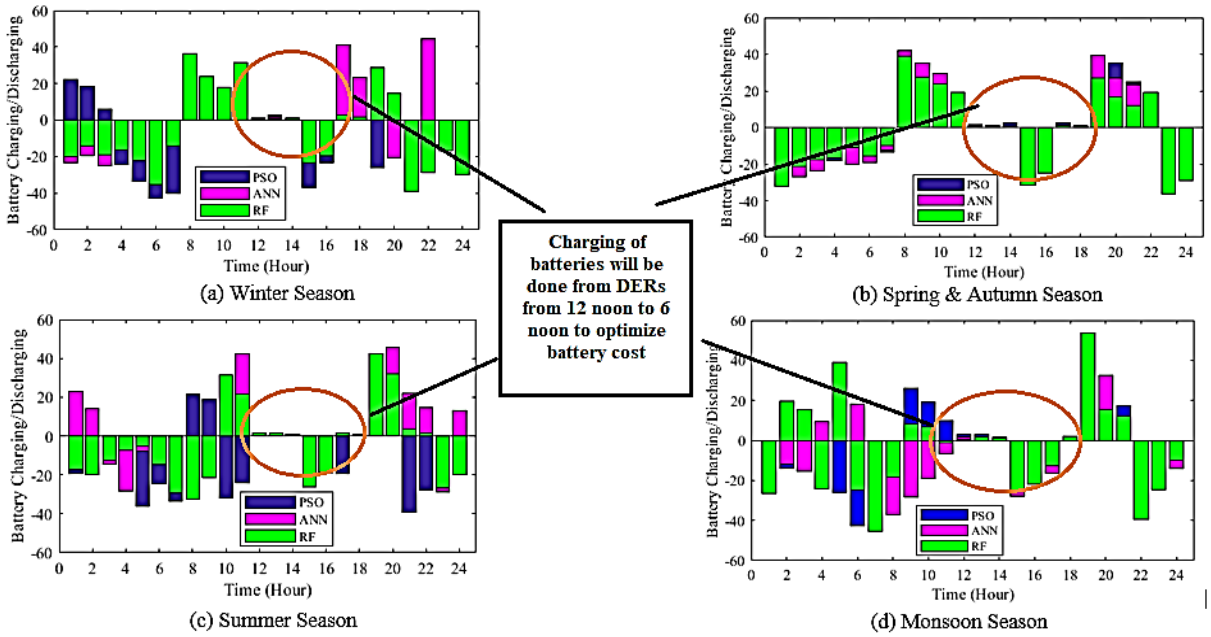

Fig. 11 Optimal battery charging and discharging state for PSO, ANN, and RF for CASE III.

5.2 Comparative Analysis between different techniques

Table 1(a)-1(c) tabulates the statistical analysis of the most efficient electrical power generation to satisfy load demand, optimal battery size, and cost minimization across different seasons. The comparison is done for population size 50 and number of iterations 100. As can be observed in CASE I from Table 1(a), the power produced by solar and wind is insufficient to meet the load requirement because of their intermittent nature. As a result, the main grid and battery storage are used to meet load demand. In this instance, the grid is used to supply the energy.

The battery must meet the minimal SOC requirement. The battery will therefore charge from RESs during off-peak hours taking into account the limits if that condition is violated. It can be seen from Tables 1(b) and 1(c) that for CASE II and CASE III, load demand can be able to meet from FC, MT, and DERs. The excess power left can be further used in EV charging or storing power in batteries. However, the cost of MT and FC systems increases which itself increases the MG system cost as the cost of thermal heat and hydrogen also increases. Therefore, the MG system only based on FC and MT cannot able to function properly in CASE II. Thus, the MG system with all DERs considered in Case III gives optimized results for RF when compared with CASE I and CASE II.

Table 1(a) Comparative Analysis of Cost for different techniques for CASE I.

Seasons	Techniques	Total Power generated from RESs (MW)	Total Load demand (MW)	Remaining load to be fulfilled (MW)	Optimal size of Battery (MWh)	Cost of power purchased from grid (Rs in Thousand/MW)	Total cost of power generated (DERs) (Rs in Thousand/MW)	Reduction in Battery (charging) cost (Rs/MWh)
Winter	PSO	216298	217717	1419	8401	155.86	155.50	1957
	ANN	213258	217717	4458	8383	162.52	167.57	1710
	RF	215718	217717	1999	8221	153.37	153.18	1853
Spring & Autumn	PSO	205300	206750	1450	8522	147.84	267.39	2113
	ANN	204758	206750	1992	8499	150.53	273.44	2227
	RF	205401	206750	1349	8326	147.91	260.09	2026
Summer	PSO	237684	239512	1829	9882	170.82	290.45	2650
	ANN	235733	239512	3779	9894	185.63	299.66	2182
	RF	237965	239512	1548	9701	170.08	286.68	2036
Monsoon	PSO	202011	203749	1737	8985	145.69	265.41	2580
	ANN	201572	203749	2176	8859	148.37	261.15	2552
	RF	202499	203749	1249	8761	142.58	248.68	2417

Table 1(b) Comparative Analysis of Cost for different techniques for CASE II.

Seasons	Techniques	Total Power generated from RESs (MW)	Total Load demand (MW)	Excess Power generated (MW)	Optimal size of Battery (MWh)	Cost of power sent to grid (Rs. In Thousand/MW)	Total cost of power generated (DERs) (Rs. In Thousand/MW)	Reduction in Battery (charging) cost (Rs/MWh)
Winter	PSO	219917	217717	-2200	8435	155.8612	155.1086	2102
	ANN	220097	217717	-2380	8438	163.9933	152.9662	1903
	RF	219843	217717	-2126	8245	157.0669	160.7745	1746
Spring & Autumn	PSO	206383	206750	987	8421	147.8412	267.4925	2570
	ANN	205863	206750	887	8512	213.8181	276.7622	2740
	RF	208560	206750	-1810	8399	159.3259	268.4109	2011
Summer	PSO	241759	239512	-2247	9895	170.8242	289.4276	2379
	ANN	241640	239512	-2128	9890	174.7256	286.3348	2286
	RF	243355	239512	-3843	9662	177.7994	282.4265	2169
Monsoon	PSO	206707	203749	-2568	9024	145.6853	265.0751	2555
	ANN	206780	203749	-2641	9121	152.523	269.8578	2154
	ANN	206959	203749	-2820	8892	159.2168	247.4122	2002

Table 1(c) Comparative Analysis of Cost for different techniques for Case III.

Seasons	Techniques	Total Power generated from RESs (MW)	Total Load demand (MW)	Excess Power generated (MW)	Optimal size of Battery (MWh)	Cost of power sent to grid (Rs. In Thousand/MW)	Total cost of power generated (DERs) (Rs. In Thousand/MW)	Reduction in Battery (charging) cost (Rs/MWh)
Winter	PSO	220809	217717	-3092	8411	155.8612	154.3606	1892
	ANN	219710	217717	-1993	8374	156.6234	157.5192	1539
	RF	221179	217717	-3462	8063	169.3762	153.0113	1384
Spring & Autumn	PSO	209551	206750	-2801	8527	157.8412	266.7699	2238
	ANN	208068	206750	-1318	8465	151.9771	260.9697	2140
	RF	209796	206750	-3046	8137	161.8798	254.9887	1982
Summer	PSO	240124	239512	-611	9406	170.8242	289.5742	3067
	ANN	240702	239512	-1190	9730	175.4285	297.7568	2809
	RF	242252	239512	-2739	9594	183.7134	254.9107	1919
Monsoon	PSO	206527	203749	-2778	8325	145.6853	264.2635	2940
	ANN	205644	203749	-1896	8349	142.6437	244.2598	2693
	RF	206778	203749	-3030	8510	152.7024	223.441	1980

5.2.1 Optimal Cost Analysis

Figure 12(a)-12(b) shows the pictorial representation of the comparison between optimal costs obtained from various strategies applied to the MG system. The annual optimal cost spent in power generation for different cases is depicted in Fig. 12(a) and Fig. 12 (b) shows the reduction in battery charging cost using various techniques for different seasons. As can be seen from Fig. 12(a) and statistical table analysis the optimal cost obtained from the RF technique gives minimal cost for all the seasons considered for different cases. Figure 12(b) clearly shows that the RF technique gives an optimal reduction in battery charging cost when constraints are implemented on it. During the winter season cost is minimal as in the case of the summer season cost increases with an increase in demand.

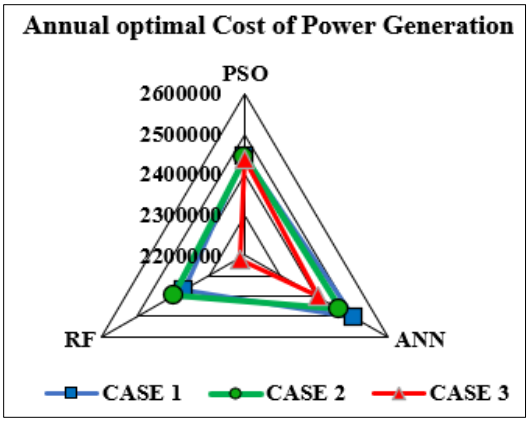

(a) Annual optimal cost of Total Power Generation.

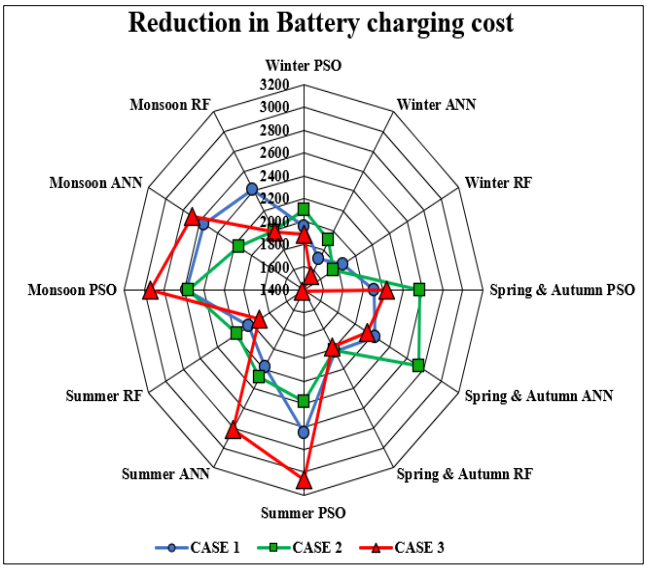

(b) Reduction in Battery charging cost

Fig. 12 Comparison between optimal cost analysis of power generation and reduction in battery charging cost using various techniques for different seasons.

5.2.2 Optimal Battery Size Analysis

The research also focuses on the estimation of optimal battery size for all the cases. The annual revenue spent on the battery size is minimal for CASE III when all the DERs are considered for optimization whereas the PSO and ANN give varied results. Figure 13 shows the comparison between average battery size (i.e. for different seasons) estimated for the different CASES using RF, ANN, and PSO techniques.

The findings demonstrate that for CASE III, the optimal battery size, reduction in battery charging cost, and cost of total power generation accomplished through the RF approach deliver the most beneficial results as compared to ANN and PSO.

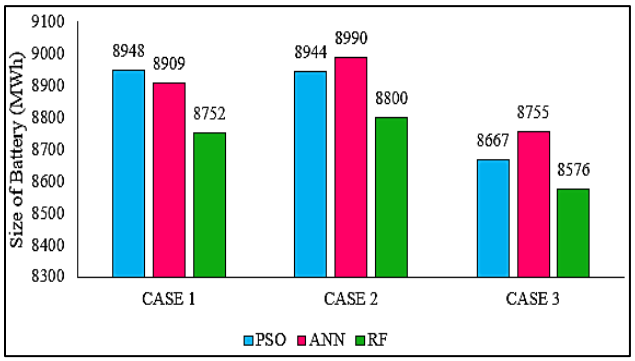

(c)

Fig. 13 Comparison between optimal battery size required in different cases using various techniques.

6 Conclusion

Electricity generation, distribution, and consumption could be completely transformed by a grid-connected microgrid system with distributed energy resources (DERs). Microgrids can offer dependable and affordable power to communities while lowering carbon emissions and boosting grid resilience by using the advantages of DERs, such as solar PV, wind turbines, and energy storage devices. Grid-connected microgrids can smoothly integrate with the current utility grid, enabling the two systems to operate together in harmony, by using modern control algorithms and communication technology. This allows for optimal utilization of DERs and ensures that power is delivered to consumers in the most efficient manner possible. In this paper, a case study using real-time load data of various seasons is optimized using the Ensemble learning-based RF technique. The optimal battery size, reduction in battery charging cost, and minimized cost of the proposed MG system with DERs are also obtained. The finding demonstrates the condition of load demand can be fulfilled by proper sizing of the battery for the considered MG system using the RF technique.

Acknowledgment

The author wants to acknowledge the Late Dr. Stuti Shukla Datta for her support and contributions to this research work.

REFERENCES

[1] Faccio, M., Gamberi, M., Bortolini, M. et al. State-of-art review of the optimization methods to design the configuration of hybrid renewable energy systems (HRESs). Front. Energy 12, 591–622 (2018). https://doi.org/10.1007/s11708-018-0567-x.

[2] Fodhil F, Hamidat A, Nadjemi O. Potential, optimization and sensitivity analysis of photovoltaic-diesel-battery hybrid energy system for rural electrification in Algeria. Energy Feb. 2019; 169:613–24. https://doi.org/10.1016/j.energy.2018.12.049.

[3] Yan Cao, Melika S. Taslimi, Sajad Maleki Dastjerdi, Pouria Ahmadi, Mehdi Ashjaee, Design, dynamic simulation, and optimal size selection of a hybrid solar/wind and battery-based system for off-grid energy supply, Renewable Energy, Volume 187, 2022, Pages 1082-1099, ISSN 0960-1481, https://doi.org/10.1016/j.renene.2022.01.112.

[4] Dalila Fares, Mohamed Fathi, Saad Mekhilef, Performance evaluation of metaheuristic techniques for optimal sizing of a stand-alone hybrid PV/wind/battery system, Applied Energy, Volume 305, 2022, 117823, ISSN 0306-2619, https://doi.org/10.1016/j.apenergy.2021.117823.

[5] Barun K. Das, Mahmudul Hasan, Fazlur Rashid, Optimal sizing of a grid-independent PV/diesel/pump-hydro hybrid system: A case study in Bangladesh, Sustainable Energy Technologies and Assessments, Volume 44, 2021, 100997, ISSN 2213-1388, https://doi.org/10.1016/j.seta.2021.100997.

[6] Olatomiwa L, Mekhilef S, Ismail MS, Moghavvemi M. Energy management strategies in hybrid renewable energy systems: A review. Renew Sustain Energy Rev Sep. 2016; 62:821–35. https://doi.org/10.1016/j.rser.2016.05.040.

[7] Shunli Wang, Carlos Fernandez, Chunmei Yu, Yongcun Fan, Wen Cao, Daniel-Ioan Stroe, A novel charged state prediction method of the lithium ion battery packs based on the composite equivalent modeling and improved splice Kalman filtering algorithm, Journal of Power Sources, Volume 471, 2020, 228450, ISSN 0378-7753, https://doi.org/10.1016/j.jpowsour.2020.228450.

[8] Y. E. García Vera, R. Dufo-López, and J. L. Bernal-Agustín, "Energy Management in Microgrids with Renewable Energy Sources: A Literature Review," *Applied Sciences*, vol. 9, no. 18, p. 3854, Sep. 2019, doi: 10.3390/app9183854.

[9] Kumar, S., Sharma, S., Sood, Y.R. et al. A Review on different Parametric Aspects and Sizing Methodologies of Hybrid Renewable Energy System. J. Inst. Eng. India Ser. B 103, 1345–1354 (2022). https://doi.org/10.1007/s40031-022-00738-2.

[10] Aeidapu Mahesh, Gangireddy Sushnigdha, Optimal sizing of photovoltaic/wind/battery hybrid renewable energy system including electric vehicles using improved search space reduction algorithm, Journal of Energy Storage, Volume 56, Part A, 2022, 105866, ISSN 2352-152X, https://doi.org/10.1016/j.est.2022.105866.

[11] Xing Qinhao, Cheng Meng, Liu Shuran, Xiang Qianliang, Xie Hailian, Chen Tailai "Multi-Objective Optimization and Dispatch of Distributed Energy Resources for Renewable Power Utilization Considering Time-of-Use Tariff", Frontiers in Energy Research, vol 9, 2021, https://www.frontiersin.org/articles/10.3389/fenrg.2021.647199, doi: 10.3389/fenrg.2021.647199, ISSN=2296-598X.

[12] Maulik, A., Das, D.: Optimal operation of microgrid using four different optimization techniques. Sustain. Energy Technol. Assess. 21, 100–120 (2017).

[13] Shah, P., Mehta, B. Microgrid Optimal Scheduling with Renewable Energy Sources Considering Islanding Constraints. Iran J Sci Technol Trans Electr Eng 44, 805–819 (2020). https://doi.org/10.1007/s40998-019-00254-y.

[14] Murty, V.V.S.N., Kumar, A. Multi-objective energy management in microgrids with hybrid energy sources and battery energy storage systems. Prot Control Mod Power Syst 5, 2 (2020). https://doi.org/10.1186/s41601-019-0147-z.

[15] Yifan Wei, Tianyi Han, Shuoqi Wang, Yudi Qin, Languang Lu, Xuebing Han, Minggao Ouyang, an efficient data-driven optimal sizing framework for photovoltaics-battery-based electric vehicle charging microgrid, Journal of Energy Storage, Volume 55, Part C, 2022, 105670, ISSN 2352-152X, https://doi.org/10.1016/j.est.2022.105670.

[16] Mohammad Amini, Amir Khorsandi, Behrooz Vahidi, Seyed Hossein Hosseinian, Ali Malakmahmoudi, Optimal sizing of battery energy storage in a microgrid considering capacity degradation and replacement year, Electric Power Systems Research, Volume 195,2021,107170, ISSN 0378-7796, https://doi.org/10.1016/j.epsr.2021.107170.

[17] Sauer D, Teodorescu R, Stan A et al. (2014) Selection and performance-degradation modeling of LiMO2/Li4Ti5O12 and LiFePO4/C battery cells as suitable energy storage systems for grid integration with wind power plants: an example for the primary frequency regulation service. IEEE Transactions on Sustainable Energy 5:90-101. doi: 10.1109/tste.2013.2273989.

[18] Robert, F C, and Gopalan S (2018) Low cost, highly reliable rural electrification through a combination of grid extension and local renewable energy generation. Sustainable Cities and Society https://doi.org/10.1016/j.scs.2018.02.010.

[19] Wilson E, Bielicki J, Pollak M et al. (2014) Why market rules matter: optimizing pumped hydroelectric storage when compensation rules differ. Energy Economics 46:10-19. doi: 10.1016/j.eneco.2014.08.017.

[20] Choi M, Kim S, Seo S (2012) Energy management optimization in a battery/supercapacitor hybrid energy storage system. IEEE Transactions on Smart Grid 3:463-472. doi: 10.1109/tsg.2011.2164816.

[21] Solomon A, Kammen D, Callaway D (2016) Investigating the impact of wind–solar complementarities on energy storage requirement and the corresponding supply reliability criteria. Applied Energy 168:130-145. doi: 10.1016/j.apenergy.2016.01.070.

[22] Robert F, Sisodia G, Gopalan S (2017) The critical role of anchor customers in rural microgrids, impact of load factor on energy cost. Sixth Int. Conf. on computation of power, energy, information and communication.

[23] Gkatzikis L, Iosifidis G, Koutsopoulos I, Tassiulas L (2014) Collaborative placement and sharing of storage resources in the smart grid. 2014 IEEE International Conference on Smart Grid Communications (SmartGridComm).

[24] Farah S, Whaley D, Pudney P, Saman W (2015) Control strategies of domestic electrical storage for reducing electricity peak demand and life cycle cost. 3rd Inter. Renewable and Sustainable Energy Conf. (IRSEC).

[25] Saffari M, De Gracia A., Fernández C, Belusko M, Boer D, and Cabeza L F (2018) Optimized demand side management (DSM) of peak electricity demand by coupling low temperature thermal energy storage (TES) and solar PV, Applied Energy, 211: 604-616, ISSN 0306-2619, https://doi.org/10.1016/j.apenergy.2017.11.063.

[26] Agamah S. U., Ekonomou L (2017) Energy storage system scheduling for peak demand reduction using evolutionary combinatorial optimisation, Sustainable Energy Technologies and Assessments, 23: 73-82, ISSN 2213-1388, https://doi.org/10.1016/j.seta.2017.08.003.

[27] Giallanza A, Porretto M, Puma GL, Marannano G. A sizing approach for stand-alone hybrid photovoltaic-wind-battery systems: A Sicilian case study. J Clean Prod oct. 2018; 199:817–30. https://doi.org/10.1016/j.jclepro.2018.07.223.

[28] Lian J, Zhang Y, Ma C, Yang Y, Chaima E. A review on recent sizing methodologies of hybrid renewable energy systems. Energy Convers Manag 2019; 199:112027. https://doi.org/10.1016/j.enconman.2019.112027.

[29] Seyed Mehdi Hakimi, Arezoo Hasankhani, Miadreza Shafie-khah, Mohamed Lotfi, João P.S. Catalão, Optimal sizing of renewable energy systems in a Microgrid considering electricity market interaction and reliability analysis, Electric Power Systems Research, Volume 203, 2022, 107678, ISSN 0378-7796, https://doi.org/10.1016/j.epsr.2021.107678.

[30] Li R, Guo Su, Yang Y, Liu D. Optimal sizing of wind/ concentrated solar plant/electric heater hybrid renewable energy system based on two-stage stochastic programming. Energy 2020; 209:118472. https://doi.org/10.1016/j.energy.2020.118472.

[31] Mayer MJ, Szil´agyi A, Gr´of G. Environmental and economic multi-objective optimization of a household level hybrid renewable energy system by genetic algorithm. Appl Energy 2020; 269:115058. https://doi.org/10.1016/j. apenergy.2020.115058.

[32] Moghaddam, S., Bigdeli, M. & Moradlou, M. Optimal design of an off-grid hybrid renewable energy system considering generation and load uncertainty: the case of Zanjan city, Iran. SN Appl. Sci. 3, 732 (2021). https://doi.org/10.1007/s42452-021-04718-x

[33] Fayza S. Mahmoud, Ahmed A. Zaki Diab, Ziad M. Ali, Abou-Hashema M. El-Sayed, Thamer Alquthami, Mahrous Ahmed, Husam A. Ramadan, Optimal sizing of smart hybrid renewable energy system using different optimization algorithms, Energy Reports, Volume 8, 2022, Pages 4935-4956, ISSN 2352-4847, https://doi.org/10.1016/j.egyr.2022.03.197.

[34] Abdelkader A, Rabeh A, Mohamed Ali D, Mohamed J. Multi-objective genetic algorithm based sizing optimization of a stand-alone wind/PV power supply system with enhanced battery/supercapacitor hybrid energy storage. Energy 2018;163: 351–63. https://doi.org/10.1016/j.energy.2018.08.135.

[35] Zhang W, Maleki A, Rosen MA, Liu J. Sizing a stand-alone solar-wind-hydrogen energy system using weather forecasting and a hybrid search optimization algorithm. Energy Convers Manag Jan. 2019; 180:609–21. https://doi.org/10.1016/j.enconman.2018.08.102.

[36] Kaabeche A, Bakelli Y. Renewable hybrid system size optimization considering various electrochemical energy storage technologies. Energy Convers Manag Aug. 2019; 193:162–75. https://doi.org/10.1016/j.enconman.2019.04.064.

[37] Xu X, Hu W, Cao D, Huang Q, Chen C, Chen Z. Optimized sizing of a standalone PV-wind-hydropower station with pumped-storage installation hybrid energy system Renew Energy Mar. 2020;147:1418–31. https://doi.org/10.1016/j. renene.2019.09.099.

[38] Bandopadhyay J, Roy PK. Application of hybrid multi-objective moth flame optimization technique for optimal performance of hybrid micro-grid system. Appl Soft Comput 2020; 95:106487. https://doi.org/10.1016/j.asoc.2020.106487.

[39] Franck Christian M. HVDC circuit breakers: a review identifying future research needs. IEEE Trans Deliv 2011; 26:998–1007.

[40] Hatziargyriou Nikos. Microgrids: architectures and control. Chichester, West Sussex, United Kingdom: Wiley-IEEE Press; 2014. p. 12–22.

[41] Che L, Khodayar ME, Shahidehpour M. Adaptive protection system for microgrids: protection practices of a functional microgrid system. IEEE ElectrMag 2014; 2:67–80.

[42] Blake, Sean T.; O'Sullivan, Dominic T.J. (2018). Optimization of Distributed Energy Resources in an Industrial Microgrid. Procedia CIRP, 67(), 104–109. doi: 10.1016/j.procir.2017.12.184.

[43] Wei M, Hong S, Alam M. An IoT-based energy-management platform for industrial facilities. Appl. Energy 2016; 164:607–619.

[44] Liu Y, Xin H, Wang Z, Gan D. Control of virtual power plant in microgrids: a coordinated approach based on photovoltaic systems and controllable loads. IET Generation, Transmission and Distribution 2015; 9:921–928.

[45] Michael Angelo Pedrasa, Ted Spooner. A survey of techniques used to control microgrid generation and

storage during island operation. In: Proceedings of the AUPEC. Melbourne, Australia; December 2006.
[46] Carrasco JM, Franquelo LG, Bialasiewicz JT, Galvan E, Guisado RCP, Prats MAM, Leon JI, Moreno-Alfonso N. Power electronic systems for the grid integration of renewable energy sources: a survey. IEEE Transactions on Power Electronics 2006;53(4):1002–16.
[47] Basak, Prasenjit; Chowdhury, S.; Halder nee Dey, S.; Chowdhury, S.P. (2012). A literature review on integration of distributed energy resources in the perspective of control, protection and stability of microgrid. Renewable and Sustainable Energy Reviews, 16(8), 5545–5556. doi: 10.1016/j.rser.2012.05.043.
[48] Quiggin D, Cornell S, Tierney M, Buswell R. A simulation and optimisation study: Towards a decentralised microgrid, using real world fluctuation data. Energy 2012; 41:549–559.
[49] Lyden, S.; Haque, M.E. (2015). Maximum Power Point Tracking techniques for photovoltaic systems: A comprehensive review and comparative analysis. Renewable and Sustainable Energy Reviews, 52(), 1504–1518. doi: 10.1016/j.rser.2015.07.172.
[50] AbdelHady, Rameen (2017). Modeling and simulation of a micro grid-connected solar PV system. Water Science, (), S1110492917300073–. doi: 10.1016/j.wsj.2017.04.001.
[51] Rezvani, Alireza; Izadbakhsh, Maziar; Gandomkar, Majid (2016). Microgrid dynamic responses enhancement using artificial neural network-genetic algorithm for photovoltaic system and fuzzy controller for high wind speeds. International Journal of Numerical Modelling: Electronic Networks, Devices and Fields, 29(2), 309–332. doi:10.1002/jnm.2078.
[52] Makbul A.M. Ramli, H.R.E.H. Bouchekara, Abdulsalam S. Alghamdi, Optimal sizing of PV/wind/diesel hybrid microgrid system using multi-objective self-adaptive differential evolution algorithm, Renewable Energy, Volume 121, 2018, Pages 400-411, ISSN 0960-1481, https://doi.org/10.1016/j.renene.2018.01.058.
[53] Ahmad Ghasemi, Mehdi Enayatzare, Optimal energy management of a renewable-based isolated microgrid with pumped-storage unit and demand response, Renewable Energy, Volume 123, 2018, Pages 460-474, ISSN 0960-1481, https://doi.org/10.1016/j.renene.2018.02.072.
[54] Hong, Y.; Lai, Y.; Chang, Y.; Lee, Y.; Liu, P. Optimizing capacities of distributed generation and energy storage in a small autonomous power system considering uncertainty in renewables. Energies 2015, 8, 2473–2492.
[55] Shrestha G, Goel L. A study on optimal sizing of standalone photovoltaic stations. IEEE Trans Energy Conv 1998; 13:373–8. http://dx.doi.org/10.1109/60.736323.
[56] Hongxing Yang; Wei Zhou; Lin Lu; Zhaohong Fang (2008). Optimal sizing method for stand-alone hybrid solar–wind system with LPSP technology by using genetic algorithm., 82(4), 354–367. doi: 10.1016/j.solener.2007.08.005.
[57] Wei Zhou; Hongxing Yang; Zhaohong Fang (2007). A novel model for photovoltaic array performance prediction. , 84(12), 1187–1198. doi: 10.1016/j.apenergy.2007.04.006.
[58] Yang H, Lu L, Zhou W. A novel optimization sizing model for hybrid solar-wind power generation system. Sol Energy 2007;81(1):76–84.
[59] Jianhua Jiang, Renjie Zhou, Hao Xu, Hao Wang, Ping Wu, Zhuo Wang, Jian Li, Optimal sizing, operation strategy and case study of a grid-connected solid oxide fuel cell microgrid, Applied Energy, Volume 307, 2022, 118214, ISSN 0306-2619, https://doi.org/10.1016/j.apenergy.2021.118214.
[60] Guo Zhao, Tianhua Cao, Yudan Wang, Huirui Zhou, Chi Zhang, Chenxi Wan, "Optimal Sizing of Isolated Microgrid Containing Photovoltaic/Photothermal/Wind/Diesel/Battery", International Journal of Photoenergy, vol. 2021, Article ID 5566597, 19 pages, 2021. https://doi.org/10.1155/2021/5566597
[61] El Azzaoui H, Mahmoudi M. Fuzzy-PI control of a doubly fed induction generator-based wind power system. J Theor Appl Inf Technol 2017:54–66.
[62] Li, Z., Zheng, Z., Xu, L. et al. A review of the applications of fuel cells in microgrids: opportunities and challenges. BMC Energy 1, 8 (2019). https://doi.org/10.1186/s42500-019-0008-3.
[63] Wee J-H. Contribution of fuel cell systems to co2 emission reduction in their application fields. Renew Sust Energ Rev. 2010; 14(2):735–44. https://doi.org/10.1016/j.rser.2009.10.013.
[64] Barbir, Frano (2005). PEM Fuel Cells || 3. Fuel Cell Electrochemistry, 33–72. doi:10.1016/B978-012078142-3/50004-5.
[65] O. Ouramdane, E. Elbouchikhi, Y. Amirat, and E. Sedgh Gooya, "Optimal Sizing and Energy Management of Microgrids with Vehicle-to-Grid Technology: A Critical Review and Future Trends," Energies, vol. 14, no. 14, p. 4166, Jul. 2021, doi: 10.3390/en14144166.
[66] Zhang Tao, "Robust Optimization of Micro-Grid of Natural Gas and Renewable Energies Considering Operational Performances and Flexibility, Frontiers in Energy Research, vol. 9, 2022, https://www.frontiersin.org/articles/10.3389/fenrg.2021.814356, 10.3389/fenrg.2021.814356, 2296-598X.
[67] Francesco F. Nicolosi, Jacopo C. Alberizzi, Carlo Caligiuri, Massimiliano Renzi, Unit commitment

optimization of a micro-grid with a MILP algorithm: Role of the emissions, bio-fuels and power generation technology, Energy Reports, Volume 7, 2021, Pages 8639-8651, ISSN 2352-4847, https://doi.org/10.1016/j.egyr.2021.04.020.

[68] Jigar S. Sarda, Kwang Lee, Hirva Patel, Nishita Patel, Dhairya Patel, Energy Management System of Microgrid using Optimization Approach, IFAC-PapersOnLine, Volume 55, Issue 9, 2022, Pages 280-284, ISSN 2405-8963, https://doi.org/10.1016/j.ifacol.2022.07.049.

[69] Zhao H, Wu Q, Wang C, Cheng L, Rasmussen CN. Fuzzy logic based coordinated control of battery energy storage system and dispatchable distributed generation for microgrid. J Mod Power Syst Clean Energy 2015; 3:422–8. doi:10.1007/s40565-015-0119-x.

[70] M. M. I. A. El-Rahman, "Optimization of Renewable Energy-Based Smart Micro-Grid System", in Modeling, Simulation and Optimization of Wind Farms and Hybrid Systems. London, United Kingdom: IntechOpen, 2020 [Online]. Available: https://www.intechopen.com/chapters/67925 doi: 10.5772/intechopen.87093.

[71] Hannah Fontenot, Bing Dong, Modeling and control of building-integrated microgrids for optimal energy management – A review, Applied Energy, Volume 254, 2019, 113689, ISSN 0306-2619, https://doi.org/10.1016/j.apenergy.2019.113689.

[72] Jasim Ali M., Jasim Basil H., Bureš Vladimír, A novel grid-connected microgrid energy management system with optimal sizing using hybrid grey wolf and cuckoo search optimization algorithm, Frontiers in Energy Research, vol 10, 2022, https://www.frontiersin.org/articles/10.3389/fenrg.2022.960141, DOI=10.3389/fenrg.2022.960141, ISSN=2296-598X

[73] Breiman, L., Friedman, J.H., Olshen, R.A., Stone, C.J.,1984: Classification and Regression Trees. Chapman and Hall (1984).

[74] Breiman. L, 1996, Bagging predictors Machine Learning, 24 (2), 123-140.

[75] Ying-Ying Cheng, P. P. K. Chan and Zhi-Wei Qiu, 2012, Random Forest based ensemble system for short term load forecasting, International Conference on Machine Learning and Cybernetics, pp. 52-56, doi: 10.1109/ICMLC.2012.6358885.

[76] Y. Xuan et al.,2021, Multi-Model Fusion Short-Term Load Forecasting Based on Random Forest Feature Selection and Hybrid Neural Network, IEEE Access, vol. 9, pp. 69002-69009, 2021, doi: 10.1109/ACCESS.2021.3051337.

[77] Durairaj, Danalakshmi, Wróblewski, Łukasz, Sheela, A., Hariharasudan, A. and Urbański, Mariusz. "Random forest based power sustainability and cost optimization in smart grid" Production Engineering Archives, vol.28, no.1, 2022, pp.82-92. https://doi.org/10.30657/pea.2022.28.10.

[78] Dou, C., Teng, S., Zhang, T., Zhang, B. and Ma, K. (2019), Layered management and hybrid control strategy based on hybrid automata and random forest for microgrid. IET Renewable Power Generation, 13.

[79] Load Data: https://bescom.karnataka.gov.in/page/Customer+Relations/BESCOM+Tariff/en.

[80] Weather Data: https://weatherspark.com/h/s/108998/2019/1/Historical-Weather-Summer-2019- in-Bengaluru-India#Figures-WindSpeed.

Jayati Vaish received a B. Tech degree from Integral University, Lucknow, Uttar Pradesh India in 2008 and a Master's degree from IIT Roorkee, Uttarakhand, India in 2013. Since 2014, she has been working as an Assistant Professor at Shri Ram Swaroop Memorial College of Engineering and Management, Lucknow, Uttar Pradesh, India. She is also a PhD scholar at Amity University, Uttar Pradesh, Lucknow Campus. She received the Best Project award in Electrical Engineering. Her area of interest includes Load Forecasting, Micro-Grid optimization, and PHEV.

Anil Kumar Tiwari received a B. Tech. from Thapar University, Patiala, India, a Master's degree from Pune University, India, and a Ph.D. degree in Electrical engineering from MNIT Allahabad, Uttar Pradesh, India. Since 2011 he has been working as Director of AMITY School of Engineering AMITY University Uttar Pradesh Lucknow Campus, India. He holds more than three decades of experience as a practicing engineer, researcher, and academic administrator. He has chaired numerous International and National Conferences and won numerous Best Paper awards in India and abroad.

Seethalekshmi K. received a B. Tech. from Regional Engineering College, Calicut, Kerala in 1991, and Master's degree from College of Engineering, Trivandrum, Kerala, India in 1996, and a Ph.D. degree in Electrical Engineering from IIT Kanpur, Uttar Pradesh, India, in 2011. From 2011 to 2016, she worked as a Professor at BBDNITM, Lucknow, Uttar Pradesh, India. Since 2017, she has been a Professor in the Electrical Engineering Department, IET, Lucknow, U.P., India. She is the author of many Journals and also a POSCO awardee. Her research interests include Power system dynamics and control, and Power system protection.